catalysts

MDPI

Article

Pt–Pd Bimetallic Aerogel as High-Performance Electrocatalyst for Nonenzymatic Detection of Hydrogen Peroxide

Chuxuan Pan [1,2,3,4], Yuanyuan Zheng [1,2,3,4], Jing Yang [1], Dongyang Lou [1,2,3,4], Jian Li [1,2,3,4], Yujing Sun [1,*] and Wei Liu [1,2,3,4,*]

1 School of Materials Science and Engineering, Sun Yat-sen University, Guangzhou 510006, China; panchx3@mail2.sysu.edu.cn (C.P.); zhengyy63@mail2.sysu.edu.cn (Y.Z.); yangj329@mail.sysu.edu.cn (J.Y.); loudy@mail2.sysu.edu.cn (D.L.); lijian87@mail2.sysu.edu.cn (J.L.)
2 The Key Laboratory of Low-Carbon Chemistry & Energy Conservation of Guangdong Province, Sun Yat-sen University, Guangzhou 510006, China
3 Key Laboratory for Polymeric Composite and Functional Materials of Ministry of Education, Sun Yat-sen University, Guangzhou 510006, China
4 State Key Laboratory of Optoelectronic Materials and Technologies, Sun Yat-sen University, Guangzhou 510006, China
* Correspondence: sunyj55@mail.sysu.edu.cn (Y.S.); liuw226@mail.sysu.edu.cn (W.L.)

Abstract: Hydrogen peroxide (H_2O_2) plays an indispensable role in the biological, medical, and chemical fields. The development of an effective H_2O_2 detecting method is of great importance. In the present work, a series of Pt_xPd_y bimetallic aerogels and Pt, Pd monometallic aerogels were controllably synthesized by one-step gelation method. Their morphologies and compositions were characterized by transmission electron microscopy, X-ray diffraction, and X-ray photoelectron spectroscopy, and so forth. These aerogels were used as nonenzyme electrocatalysts for the detection of H_2O_2. The cyclic voltammetric and amperometric results demonstrated that the performance of the metal aerogels showed volcano-type behavior, with the $Pt_{50}Pd_{50}$ aerogel sitting on top. The $Pt_{50}Pd_{50}$ aerogel-based electrochemical sensor exhibited excellent comprehensive performance, with a low overpotential of −0.023 V vs. Ag/AgCl, a broad linear range from 5.1 to 3190 μM (R^2 = 0.9980), and a high sensitivity of 0.19 mA mM^{-1} cm^{-2}, in combination with good anti-interference ability and stability. A comprehensive study indicated that the superior sensing performance of the $Pt_{50}Pd_{50}$ aerogel is closely related to its optimized d-band center and larger cumulative pore volume. This work first applied Pt–Pd bimetallic aerogels into the detection of H_2O_2 and shows the promising application of noble metal aerogels in the electrochemical sensing area.

Keywords: electrochemical sensors; hydrogen peroxide; electrocatalysis; alloying effect

Citation: Pan, C.; Zheng, Y.; Yang, J.; Lou, D.; Li, J.; Sun, Y.; Liu, W. Pt–Pd Bimetallic Aerogel as High-Performance Electrocatalyst for Nonenzymatic Detection of Hydrogen Peroxide. *Catalysts* **2022**, *12*, 528. https://doi.org/10.3390/catal12050528

Academic Editor: Federica Menegazzo

Received: 5 April 2022
Accepted: 5 May 2022
Published: 8 May 2022

1. Introduction

Hydrogen peroxide (H_2O_2), as one of the most important reactive oxygen species (ROS) in the metabolism of organisms, is considered to be a biomarker due to its vital function in aging and disease [1,2]. H_2O_2 is not only the intermediate or final product in wide fields, such as wastewater treatment, bleaching, mining, metal processing, and other chemical engineering fields [3–5], which may cause diseases and explosion due to its oxidative and corrosive properties [6]. Therefore, developing effective and accurate methods to detect H_2O_2 is of great importance [7].

Up to now, various analytical techniques have been used to detect H_2O_2, such as spectrophotometry, electrochemistry, and chromatography [8,9]. Among various analytical techniques for H_2O_2 detection, the electrochemical method is considered to be the most outstanding one due to its great advantages, such as simplicity, low cost, rapid response, high sensitivity, and good selectivity [10]. The core materials of electrochemical sensors are electrocatalysts, among which bimetallic nanocatalysts, such as Pd–Cu, Au–Pd,

Pt–Pd, Au–Pt, and Pt-Ni, with various morphologies or supported on various supporting materials have been investigated extensively for sensing H_2O_2 [11–18], because of their prominent electronic and catalytic properties over their monometallic counterparts resulting from the synergetic effect [19]. Despite great efforts made, it is still a great challenge for such materials to meet simultaneously the requirements of electrochemical sensors for practical application from the points of view of low detection limit, broad linear range, high sensitivity, good selectivity, good reproducibility, and good stability.

Noble metal aerogels (NMAs) own unique three-dimensional (3D) self-supported solid networks with interconnected macropores or mesopores filled with air [20]. Combining the structural features of aerogels and physicochemical properties of noble metals, the NMAs simultaneously combine numerous active sites, rapid electron transfer paths, and fast mass transport channels, which render them highly effective electrocatalysts [21]. Although NMAs have distinguished themselves in electrocatalysis [22–32] (e.g., methanol/ethanol oxidation reaction (M/EOR), carbon dioxide reduction reaction (CO_2RR), oxygen reduction reaction (ORR), formic acid oxidation, glucose oxidation), using them as electrochemical nanocatalysts for H_2O_2 detection is still in its infancy, and a lot more treasures need researchers to unlock.

Here, electrochemical sensors for direct detection of H_2O_2 were fabricated by Pt, Pd monometallic, and Pt_xPd_y bimetallic aerogels ($Pt_{20}Pd_{80}$, $Pt_{50}Pd_{50}$, and $Pt_{80}Pd_{20}$), which were synthesized via a simple one-step gelation method. For the first time, Pt, Pd, and Pt_xPd_y aerogels were used as electrocatalyst to detect H_2O_2. The electrochemical performance of the Pt, Pd, and Pt_xPd_y aerogels showed volcano-type behavior, with the $Pt_{50}Pd_{50}$ aerogel sitting on top. The $Pt_{50}Pd_{50}$ aerogel-based electrochemical sensor exhibited excellent comprehensive performance for the detection of H_2O_2, with a low overpotential of −0.023 V vs. Ag/AgCl, a broad linear range from 5.1 to 3190 μM (R^2= 0.9980), and a high sensitivity of 0.19 mA mM^{-1} cm^{-2}, in combination with good stability and good anti-interference ability.

2. Results

2.1. Physicochemical Properties of Pt_xPd_y Bimetallic Aerogels and Pt, Pd Monometallic Aerogels

The Pt_xPd_y bimetallic aerogels and the Pt and Pd monometallic aerogels were prepared through a simple one-step gelation method, followed by supercritical drying, as shown in Scheme 1. The morphologies of the catalysts used in the H_2O_2 sensor fabrication was characterized by transmission electron microscopy (TEM). As shown in Figure 1, the Pt_xPd_y aerogels with different constituents and the Pt and Pd monometallic aerogels all have semblable porous three-dimensional network structures with interconnected metal nanowires. The average diameters of the ligaments are 4.4 ± 1.3, 4.4 ± 1.2, 4.9 ± 1.3, 4.6 ± 1.6, and 7.4 ± 2.0 nm for the Pt aerogel, $Pt_{80}Pd_{20}$ aerogel, $Pt_{50}Pd_{50}$ aerogel, $Pt_{20}Pd_{80}$ aerogel, and Pd aerogel, respectively. The corresponding statistical histogram is shown in Figure S1.

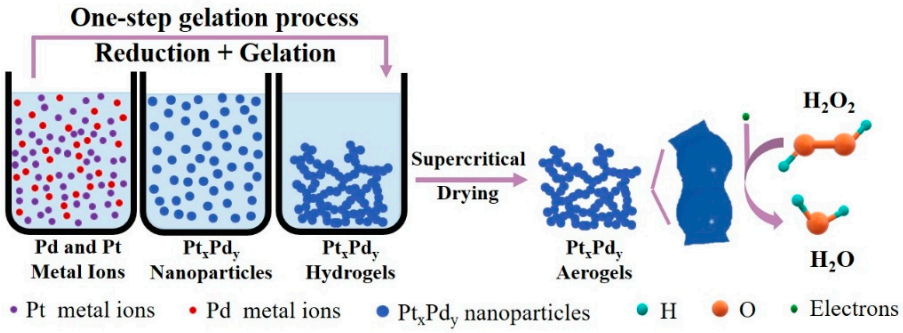

Scheme 1. Schematic illustration of the synthesis of Pt_xPd_y aerogels for electrochemical sensing of H_2O_2.

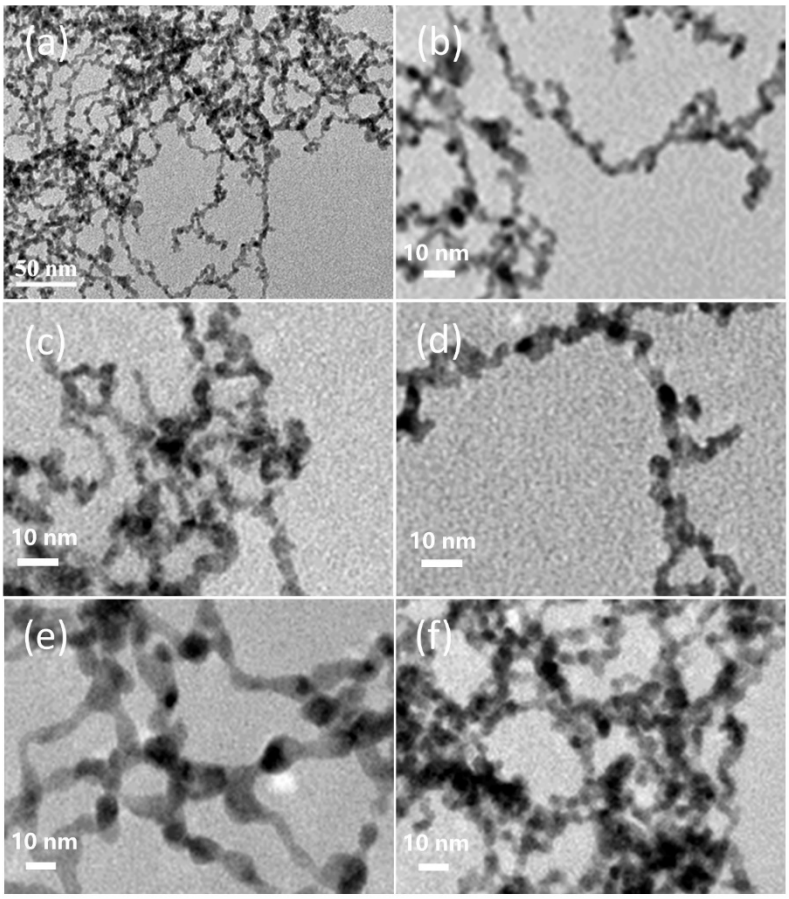

Figure 1. TEM images of (**a**,**b**) $Pt_{50}Pd_{50}$, (**c**) $Pt_{20}Pd_{80}$, (**d**) $Pt_{80}Pd_{20}$, (**e**) Pd, and (**f**) Pt aerogels.

X-ray diffraction (XRD) was used to reveal the crystalline structures of the aerogels, and the results are shown in Figure 2a; the diffraction peaks at about 39°, 46°, 67°, 81°, and 86° corresponded with the (111), (200), (220), (311), and (222) planes of the face-centered cubic (fcc) structure of Pt and Pd (JCDPS card No.: 04-0802 and No.: 46-1043), respectively. As the metal Pt and Pd have the same crystal structure and a small lattice mismatch (Pt: a = 3.93 Å; Pd: a = 3.89 Å), the diffraction peaks of the two metals are overlapped. However, as observed from Figure 2a, the diffraction peaks shift slightly to the right with the increasing proportion of Pd in the Pt_xPd_y bimetallic aerogels. This can be ascribed to the smaller lattice constant of Pd, which is incorporated into the lattice of Pt, leading to the decreased cell parameters and crystal plane spacing, which may introduce compressive strain [33]. It has been previously reported that the appropriate strain existing in Pt-based alloy systems can optimize the Pt d-band center and therefore enhance the catalytic activity [34].

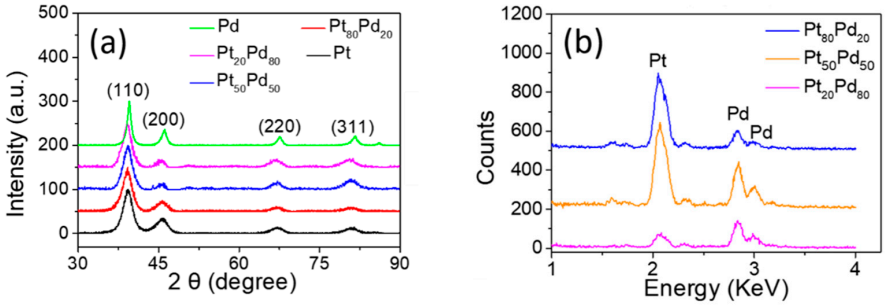

Figure 2. (**a**) XRD spectra of Pt_xPd_y bimetallic and Pt, Pd monometallic aerogels. (**b**) TEM–EDS of $Pt_{80}Pd_{20}$, $Pt_{50}Pd_{50}$, and $Pt_{20}Pd_{80}$ aerogels.

Energy dispersive spectroscopy (EDS) (Figure 2b) and X-ray photoelectron spectroscopy (XPS) (Figure 3a–f) were used to reveal the composition and surface electronic properties of bimetallic aerogels, respectively. The results are summarized in Table 1. It can be seen that the compositions of bimetallic aerogels are in good agreement with the feed ratio.

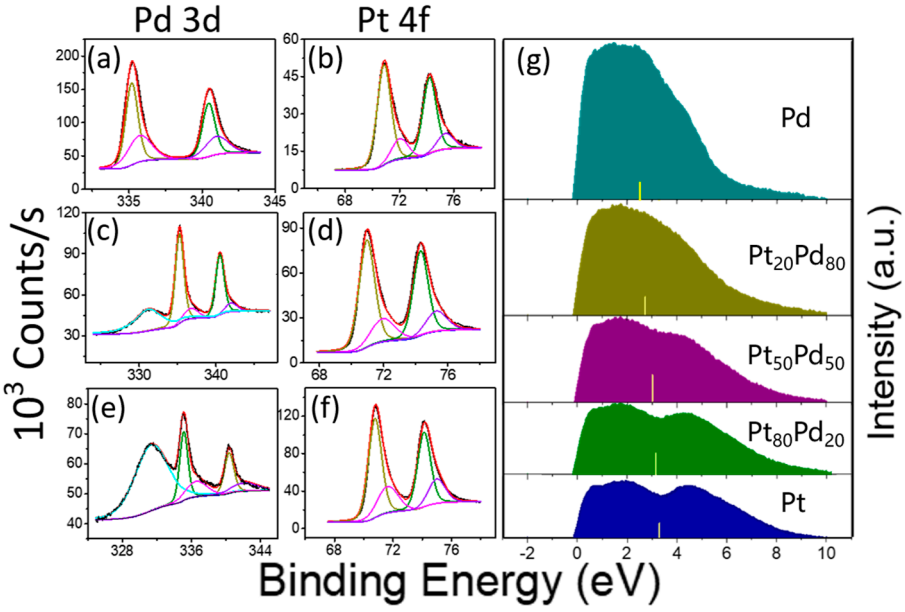

Figure 3. XPS spectra of (**a**,**b**) $Pt_{20}Pd_{80}$, (**c**,**d**) $Pt_{50}Pd_{50}$, and (**e**,**f**) $Pt_{80}Pd_{20}$ aerogels; (**g**) surface valance band spectra of the Pt, Pd monometallic aerogels and Pt_xPd_y bimetallic aerogels. All the spectra were corrected using a Shirley background. The yellow bars indicate the location of the d-band center.

Table 1. Molar ratio of Pt/Pd and metal/metal oxides in the Pt_xPd_y aerogels revealed from EDS and XPS and location of the d-band center of all the aerogels.

Aerogels	Expected Pt/Pd (at%)	EDS Pt/Pd (at%)	XPS (at%)			D-Band Center Location (eV)
			Pt/Pd	Pt/PtO	Pd/PdO	
Pd	0/100	-	-	-	57.3/42.7	2.47
$Pt_{20}Pd_{80}$	20/80	20.4/79.7	24.9/75.1	80.2/19.8	62.0/38.0	2.74
$Pt_{50}Pd_{50}$	50/50	50.6/49.4	59.6/40.4	75.2/24.8	83.7/16.3	3.02
$Pt_{80}Pd_{20}$	80/20	83.2/16.8	85.7/14.3	70.2/29.8	64.3/35.7	3.11
Pt	100/0	-	-	83.3/16.7	-	3.27

The high-resolution Pd 3d and Pt 4f XPS spectra are shown in Figure 3a–f. Obviously, Pt 4f spectra can be deconvoluted into four peaks: Pt $4f_{7/2}$ and Pt $4f_{5/2}$ at 70.9 and 74.2 eV can be ascribed to Pt^0; meanwhile, Pt $4f_{7/2}$ and Pt $4f_{5/2}$ peaks at 72.1 and 75.4 eV correspond to Pt^{II}. Analogously, Pd 3d spectra are deconvoluted into four peaks: the peaks at 335.2 and 340.5 eV can be ascribed to Pd $3d_{5/2}$ and Pd $3d_{3/2}$ of Pd^0, respectively, while the peaks at 335.8 and 341.1 eV arose from Pd $3d_{5/2}$ and Pd $3d_{3/2}$ of Pd^{II}, respectively [30]. The peak neighboring to the Pd $3d_{5/2}$ appearing at 331 eV is Pt $4d_{3/2}$ (Figure 3c,e) [35].

The surface compositions of Pt_xPd_y and Pt, Pd aerogels were also calculated semi-quantitatively (Table 1). On the surface of Pt_xPd_y aerogels, about 20–30% Pt element is Pt^{II}, while 16–38% Pd element is Pd^{II}. The proportion of Pt in the surface region is higher than the result obtained from EDS, which may be caused by the faster reduction rate of the Pd metal salt precursor [35].

Surface valance band spectra collected by XPS were used to calculate the d-band center of the Pt, Pd monometallic aerogels and Pt_xPd_y bimetallic aerogels. It can be seen from

Figure 3g that the calculated d-band center for Pt, $Pt_{80}Pd_{20}$, $Pt_{50}Pd_{50}$, $Pt_{20}Pd_{80}$, and Pd aerogels gradually shifts down from 3.27 to 2.47 eV with the increase in Pd content.

2.2. Electrocatalytic Reduction of H_2O_2 by the Metal Aerogel Catalyst Modified Glassy Carbon Electrodes

The performance of Pt_xPd_y aerogels on glassy carbon electrodes (GCEs) toward the electrocatalytic reduction reaction of H_2O_2 (H_2O_2RR) was investigated in detail by cyclic voltammetry (CV). Figure 4a shows the electrocatalytic current response of the $Pt_{50}Pd_{50}$ sensor in the absence and presence of H_2O_2 between 0 and 2.0 mM within −0.64−0.96 V vs. Ag/AgCl. It is evident that excellent electrocatalytic response can be observed, and electrochemical reduction current at about −0.15 V gradually increased with the increasing concentration of H_2O_2.

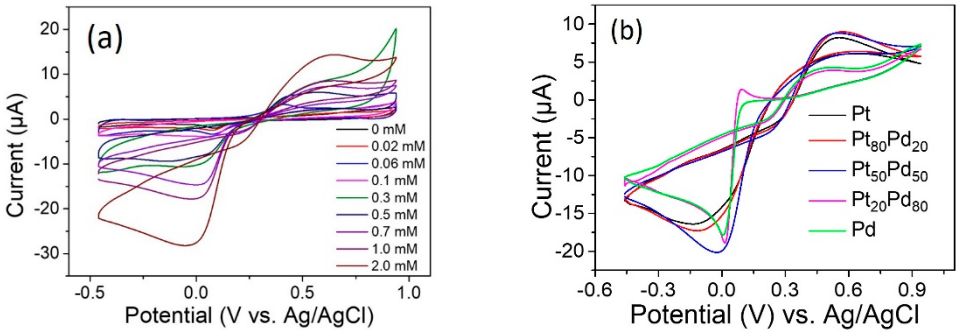

Figure 4. (**a**) CV curves of $Pt_{50}Pd_{50}$ aerogel modified GCE at concentrations of 0, 0.02, 0.06, 0.1, 0.3, 0.5, 0.7, 1.0, and 2.0 mM H_2O_2 in N_2-saturated 0.1 M phosphate buffer saline (PBS). (**b**) CV curves of bimetallic aerogels and monometallic aerogel modified GCEs at a concentration of 1.0 mM H_2O_2 in N_2-saturated 0.1 M PBS. Potential range: −0.64-0.96 V vs. Ag/AgCl. Scan rate: 50 mV s^{-1}.

Figure 4b shows the electrocatalytic responses of all the as-prepared catalysts at a concentration of 1 mM H_2O_2, and a summary of the results is shown in Table 2. It should be noted that the CV background signals in 0.1 M PBS were subtracted. Pd, $Pt_{20}Pd_{80}$, and $Pt_{50}Pd_{50}$ aerogels all display very low overpotentials at about 0.004, −0.014, and −0.023 V, respectively. However, the $Pt_{50}Pd_{50}$ aerogel displays the highest peak current, about 27 μA, while $Pt_{20}Pd_{80}$, $Pt_{80}Pd_{20}$, Pt, and Pd aerogels display 20, 23, 22, and 17 μA, respectively. The H_2O_2 reduction catalytic performances of the as-prepared aerogels show volcano-type behavior, and the superiority of the $Pt_{50}Pd_{50}$ aerogel catalyst can be ascribed to the modulated electronic structure and bimetallic synergistic effect with an optimized d-band center.

Figure S3 shows the effect of scan rates on current. The reduction peak currents were proportional to the square root of the scanning rate, and the linear regression equation is $Y = 0.98 \times X - 10.02$ ($R^2 = 0.994$). These results indicate that the electroreduction process is a diffusion-controlled process [15].

2.3. Effect of pH in H_2O_2 Detection by the $Pt_{50}Pd_{50}$ Aerogel Catalyst Modified Glassy Carbon Electrode

In electrochemical process, pH may have an important impact on the electrochemical reaction. Consequently, in our study, an experiment was conducted to evaluate this effect in H_2O_2 detection using the prepared $Pt_{50}Pd_{50}$ aerogel modified glassy carbon electrode. As part of this study, cyclic voltammetry responses of the $Pt_{50}Pd_{50}$ aerogel in PBS solutions with different pH comprising 1 mM concentration of H_2O_2 at a constant scan rate of 50 mV s^{-1} was recorded, and the result is shown in Figure 5. As we can see, the response currents display "Volcanic type" behavior, while the peak potentials have no obvious rule. The $Pt_{50}Pd_{50}$ aerogel in PBS solutions with 7.4 pH showed the highest response current and lowest peak potential. Additionally, the atmosphere of pH 7.4 provides a possibility for biological applications. Hence, we selected pH 7.4 PBS as electrolyte for further sensing performance evaluation.

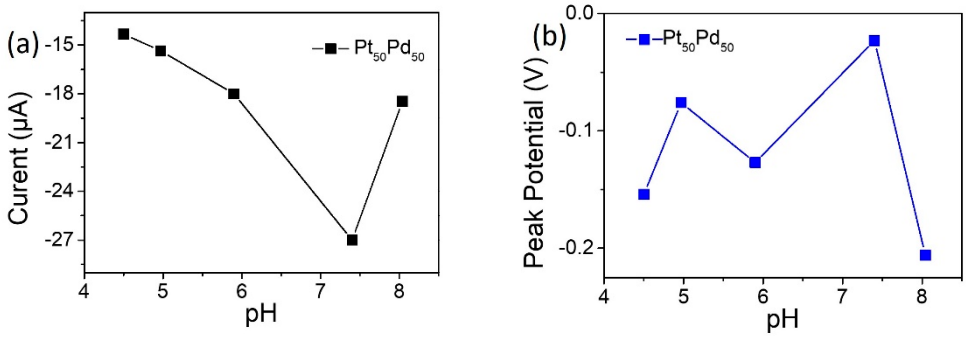

Figure 5. (**a**) CV peak currents of $Pt_{50}Pd_{50}$ in PBS solutions with different pH comprising 1 mM concentration of H_2O_2. (**b**) Peak potentials of $Pt_{50}Pd_{50}$ in PBS solutions with different pH comprising 1 mM concentration of H_2O_2.

2.4. Amperometric Sensing of H_2O_2 by Pt_xPd_y Bimetallic Aerogels and Pt, Pd Monometallic Aerogels

Figure 6 displays the current-time (i-t) responses of $Pt_{50}Pd_{50}$ aerogel and other aerogels to the successive addition of different concentrations of H_2O_2 into N_2-saturated 0.1 M PBS solution under continuous stirring at a working potential of −0.05 V. All sensors exhibit steplike linear responses, and the responses are fast and the sensors could achieve 95% of the steady-state current within about 5 s. Compared with other catalysts, the $Pt_{50}Pd_{50}$ aerogel display the highest sensitivity of 0.190 mA mM^{-1} cm^{-2} (Figure 6b) and the lowest limit of detection (LOD) of 2.21 μM on a signal-to-noise (S/N) ratio of 3, while the sensitivities of the $Pt_{80}Pd_{20}$, $Pt_{20}Pd_{80}$, Pt, and Pd aerogels are 0.160, 0.114, 0.143, and 0.047 mA mM^{-1} cm^{-2}, respectively (Figure 6c)). Their LOD ranges from 2.73 to 21.3 μM. The linear ranges of all the aerogel catalysts cover three or four orders of magnitude with a high correlation coefficient (≥0.998).

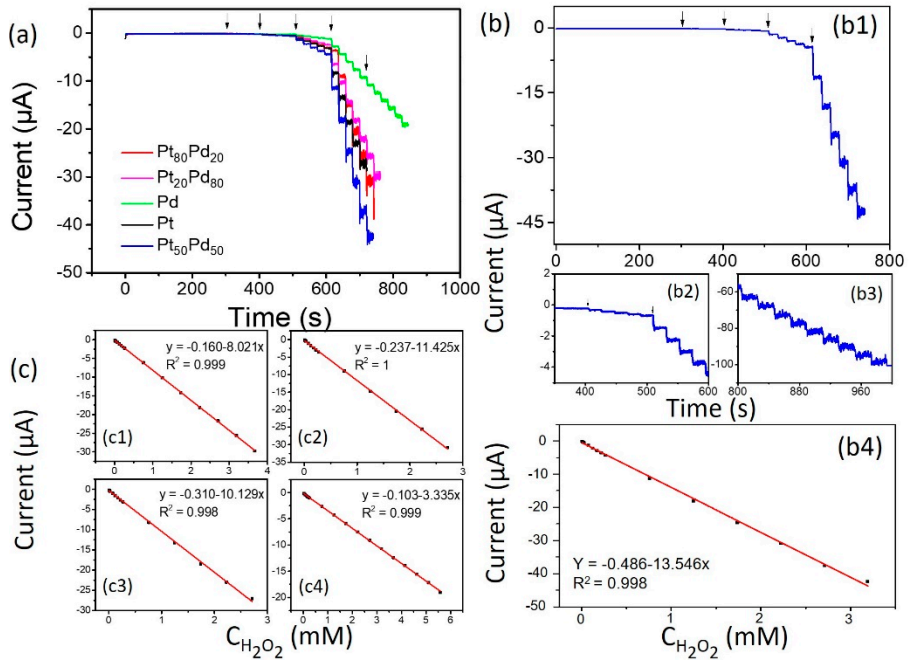

Figure 6. (**a**) Amperometric responses of the aerogel modified electrodes with successive addition of 2×10^{-5} M (50 μL), 0.002 M (50 μL), 0.02 M (50 μL), 0.6 M (17 μL), and 1 M (10 μL) into 20 mL N_2-saturated 0.1 M PBS aqueous solution at −0.05 V. (**b**) (b1) Amperometric responses of the $Pt_{50}Pd_{50}$ aerogel modified electrodes (b2,b3). Enlarged part of amperometric response of $Pt_{50}Pd_{50}$ aerogel modified electrode. (b4) Calibration curve of the $Pt_{50}Pd_{50}$ for H_2O_2RR in N_2-saturated PBS aqueous solution. (**c**) (c1–c4) Calibration curve of $Pt_{20}Pd_{80}$, $Pt_{80}Pd_{20}$, Pt, and Pd for H_2O_2RR in N_2-saturated PBS aqueous solution.

Figure 7 shows the relationship between the atom ratios of Pt and Pd in the Pt_xPd_y bimetallic aerogels and their electrochemical sensing performances, including the sensitivity, LOD, and potential of reduction peak (E_{pc}), as well as the physical properties, including the d-band center, BET surface area, and cumulative pore volume. Compared with the other as-prepared aerogel sensors, the $Pt_{50}Pd_{50}$ bimetallic aerogel-based sensor is the optimal one, showing higher sensitivity, broader linear range, and lower detection limit in H_2O_2 detection. The excellent electrocatalytic response of the $Pt_{50}Pd_{50}$ aerogel is closely related to the synergy bimetallic effect. Based on the d-band center energy theory (ε_d) [36], milder binding energy to the reaction intermedia is beneficial for the release of products and adsorption of reactants, thus leading to better catalytic performance. The appropriate downshifted d-band center of $Pt_{50}Pd_{50}$ aerogels caused by alloying effect and electronic effect might be one reason for the higher sensing performance of the $Pt_{50}Pd_{50}$ aerogel than other Pt_xPd_y aerogels [27,37]. As for the influences of BET surface area, pore size distribution, and cumulative pore volumes, it is found that there are no direct influences of BET surface area and pore size distribution [30] on sensing performance; however, the changing tendency of cumulative pore volume with Pt/Pd ratio is the same as the Pt_xPd_y aerogels' sensitivity and contrary to the onset potential. The biggest pore volume may also be one of the reasons for the better sensitivity and lower onset potential of the $Pt_{50}Pd_{50}$ aerogel than the other Pt_xPd_y aerogels. Meanwhile, the advanced structure of NMAs, including the high hierarchically porous 3D network, interconnected nanowires, faster electron and mass transport, more abundant active sites, and excellent structural stability, should be also considered.

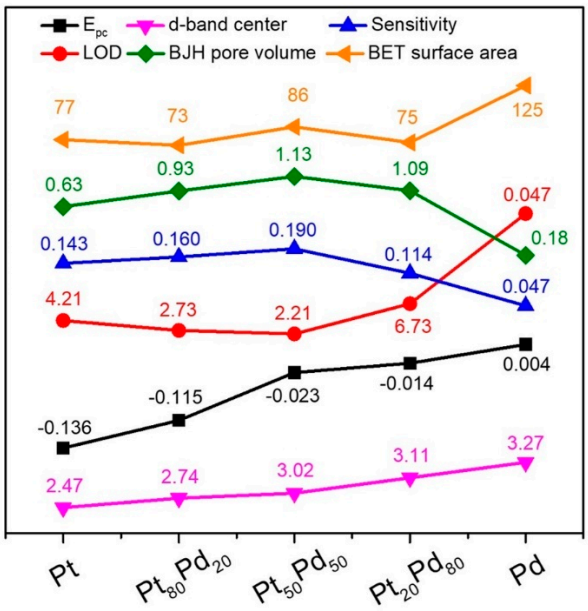

Figure 7. The relationship between the ratio of Pt and Pd in the as-prepared Pt_xPd_y aerogels and their sensitivity (mA mM^{-1} cm^{-2}), LOD (μM), E_{pc} (V), BET surface area (m^2 g^{-1}), BJH pore volume (cm^{-3} g^{-1}), and d-band center (eV).

A comparison between the as-prepared electrochemical sensors based on Pt_xPd_y bimetallic aerogels and Pt, Pd monometallic aerogels with other Pt-containing and Pd-containing monometallic or bimetallic ones reported in the literatures for the determination of H_2O_2 is shown in Table 2.

Compared with the reported Ag wire aerogel sensor [38], our Pt_xPd_y bimetallic aerogels and Pt, Pd monometallic aerogel catalysts here have a much wider linear range, a much lower working potential, and a much faster reaction rate, which may be ascribed to the more active composition of Pt and Pd bimetal with better catalytic activity and their thinner size. When compared with other reported bimetallic catalysts containing Pt and

Pd elements, the $Pt_{50}Pd_{50}$ aerogel has lower overpotential and a generally wider linear range. In the previous reports, the Pt and Pd containing catalysts are mostly combined with various supporting materials, such as graphene, carbon nanotubes, and MoS_2 [12,39,40]. Using support materials is to make use of the large specific surface area of their conductive network structure to anchor the metal catalyst particles or clusters [15,41]. However, most of the support materials have no catalytic properties, leading to slower kinetics and higher working potential. Our metal aerogel catalysts own a self-supporting metallic porous conductive network structure, which can provide a large specific surface area and a large amount of catalytic active sites, fast electron transfer and mass transport, and correspondingly a much lower overpotential and a generally wider linear range. Even though loadings of metal aerogels on electrodes are very low, the sensors can maintain generally very good sensitivity.

Table 2. Summary of the performances of the nonenzymatic H_2O_2 electrochemical sensors based on aerogel materials and Pt and Pd elements containing bimetallic materials.

Electrode	CV E_{pc} (V)	$E_{applied}$ (V vs. Ag/AgCl)	Linear Range (μM)	LOD (μM)	Sensitivity (mA mM^{-1} cm^{-2})	$t_{response}$ (s)	Substrate Materials	Ref
$Pt_{50}Pd_{50}$ aerogel	−0.023	−0.05	5.1–3190	2.21	0.19	3	-	This work
$Pt_{80}Pd_{20}$ aerogel	−0.115	−0.05	5.1–4200	2.73	0.16	2	-	This work
$Pt_{20}Pd_{80}$ aerogel	−0.014	−0.05	10–3700	6.73	0.114	3	-	This work
Pt aerogel	−0.136	−0.05	5.2–2700	4.21	0.143	≤5 s	-	This work
Pd aerogel	0.004	−0.05	19–5576	21.3	0.047	≤5 s	-	This work
Ag wire aerogel	~−0.14	−0.46	0–800	2.1	0.42	~50 s	-	[38]
Pt–Pd/CFME	not obvious	−0.4	5–3920	0.48	10.4	≤5 s	carbon fiber	[42]
Pt–Pd NPs/GO-CFMs	~−0.2	−0.2	1–35	0.3	0.98 μA mM^{-1}	-	graphene oxide sheathed carbon fiber	[43]
Pt–Pb/graphene	~−0.19	−0.2	0.002–2516	0.002	1.82, 0.91, 4.05	2	graphene	[12]
Pt (750 s) Pd/MoS_2	not obvious	−0.35	10–80	3.4	7.64	-	MoS_2	[39]
$Pt_{48}Pd_{52}$− Fe_3O_4 NPs	−0.456	−0.25	0.02–0.1 0.1–2.0 2.0–14,000	0.005	-	2	Fe_3O_4	[44]
PdPt NCs@SGN	~0.13	−0.06	1–300	0.3	14,968.75	3	SnO_2/graphene nanosheets	[41]
Pt–PdCu NCs	~0.05	0.05	1.5–1160	1.5	0.562	-	none	[45]
$[PB/WV-Pt@Pd]_6$	<−0.5	−0.3	0.4–2650	0.1	0.0551		$PW_9V_3O_{40}{}^{3-}$	[46]
Pd core–Pt NDs-rGO	~0.02	0.018	5–500	0.027	0.672	≤5 s	PDDA–rGO	[47]
Pt–Pd/IL-$rGOP_{(II)}$	−0.35	0.2 *	0.1–37.6	0.01		≤5 s	IL–graphene paper	[48] *

* Means the references in which E_{pc} is shown here in the table for comparison, while in the reference the aerometric detection of H_2O_2 was performed utilizing the oxidation of H_2O_2. All potentials listed here are referenced to or converted to be referenced to Ag/AgCl (3 M KCl). CFME: carbon fiber microelectrode; MWCNTs: multiwalled carbon nanotubes; CGE: carbon glass electrode; NPs: nanoparticles; GO: graphene oxide; CFMs: carbon fiber microelectrodes; rGO: reduced graphene oxide nanosheets; CNTs: carbon nanotubes; SPGFE: screen-printed gold nanofilm electrode; BNC: bimetallic nanoclusters; NCs: nanocages; SGN: SnO_2/graphene nanosheets; NCs: nanocages; rGOP: reduced graphene-based nanohybrid paper, Prussian blue; WV: $PW_9V_3O_{40}{}^{3-}$; NDs: nanodendrites; PDDA: poly(diallyldimethylammonium chloride); G: graphene; IL: ionic liquid (1-butyl-3-methylimidazolium tetrafluoroborate).

2.5. Selectivity, Reproducibility, Repeatability, and Stability of the As-Prepared Sensors

Selectivity is an important factor for nonenzymatic sensors. The possible interferences with H_2O_2, such as glucose (GLU), saccharose (SUC), and ascorbic acid (AA), in $Pt_{50}Pd_{50}$ aerogel were investigated. As shown in Figure 8a, after injecting 2 μM H_2O_2 into 20 mL N_2-saturated 0.1 M PBS aqueous solution, 2 mM of the above interfering materials was also

injected successively. There is no significant change and influence on the current curves and the subsequent response for another 2 μM H_2O_2 injected later.

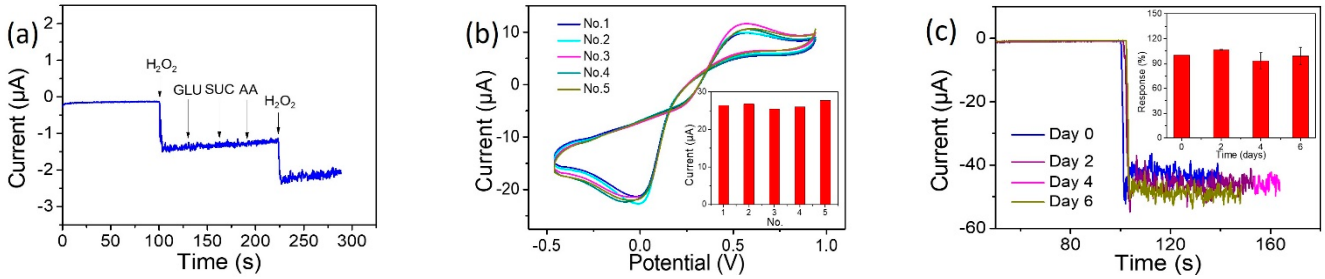

Figure 8. (**a**) The amperometric response of the $Pt_{50}Pd_{50}$ aerogel modified GCE with respective additions of 2 μM H_2O_2, 2 mM glucose, 2 mM saccharose, 2 mM ascorbic acid, and 2 μM H_2O_2 in N_2-saturated 0.1 M 20 mL PBS at −0.05 V. (**b**) The current responses of five different $Pt_{50}Pd_{50}$ aerogel modified GCEs synthesized under the same conditions at a concentration of 1 mM H_2O_2. The inset picture is the current responses calculated in the form of bar charts. (**c**) An example of stability test of one $Pt_{50}Pd_{50}$ modified GCE over 6 days in the air at room temperature. The inset picture is the current responses of three $Pt_{50}Pd_{50}$ modified GCEs over 6 days (in the air at room temperature) calculated in the form of bar charts.

Five different $Pt_{50}Pd_{50}$-modified electrodes prepared under the same conditions were used to test the reproducibility of this sensor by measuring the current responses to a concentration of 1 mM H_2O_2. Obviously, Figure 8b shows an excellent reproducibility of the aerogel sensor with the relative standard deviation (RSD) of 3.26%.

Moreover, the stability of the $Pt_{50}Pd_{50}$ aerogel sensor was also evaluated. As shown in Figure 8c, after 6 days of storage at room temperature and air atmosphere, the response current of the sensor could be kept at least at 90%. Additionally, the repeatability of the $Pt_{50}Pd_{50}$ sensors was evaluated by testing responses to continuous addition of 2 mM (50 μL) H_2O_2 into 20 mL N_2-saturated PBS. As can be seen in Figure S2, the sensor had good repeatability, and the RSD of the response current was 6.3%. These results indicate that the $Pt_{50}Pd_{50}$ aerogel sensor for detecting H_2O_2 has great selectivity, reproducibility, repeatability, and stability.

3. Materials and Methods

3.1. Reagents and Chemicals

Chloroplatinic acid hexahydrate ($H_2PtCl_6{\cdot}6H_2O$), potassium chloropalladite (K_2PdCl_4, 99.95%), sodium borohydride ($NaBH_4$, 98%), disodium hydrogen phosphate dodecahydrate ($Na_2HPO_4{\cdot}12H_2O$,99%), sodium dihydrogen phosphate dihydrate ($NaH_2PO_4{\cdot}2H_2O$), and L-ascorbic acid (AA, ≥99%) were purchased from Aladdin. D- (+) glucose (GLU) and sucrose (SUR) were obtained from Macklin. Gamma alumina powder (0.3 μm) was received from Gaoss Union. Hydrogen peroxide (30%) was bought from Guangzhou Chemical Reagent Factory. Milli-Q water (18.2 MΩ cm^{-1}) was used in the aqueous solutions through all the experiments. The phosphate buffer solution (PBS, pH = 7.4) was prepared by mixing $NaH_2PO_4{\cdot}2H_2O$ (0.1 M) and $Na_2HPO_4{\cdot}12H_2O$ (0.1 M) aqueous solution.

3.2. Synthesis of Pt_xPd_y Bimetallic Aerogels and Pt, Pd Monometallic Aerogels

NMAs were synthesized based on the reported one-step gelation method [30] with slight modification. For the bimetallic aerogels, taking the $Pt_{50}Pd_{50}$ aerogel as an example, typically, 13.0 mg K_2PdCl_4 (final reacting concentration of 0.1 mM) and 227.7 μL of 0.176 M $H_2PtCl_6{\cdot}6H_2O$ (final reacting concentration of 0.1 mM) were added to 395 mL deionized water and stirred for 10 min. Then, 5 mL of fresh 40 mM $NaBH_4$ solution (final reacting concentration of 0.5 mM) was injected rapidly into the previous mixed metallic salt aqueous solution under a disturbing ambient, and then the color of the solution changed rapidly from bright yellow to gray black. The solution was kept being stirred for another 30 min,

then settled still for about 6–12 h; a black $Pd_{50}Pt_{50}$ hydrogel would deposit at the bottom of the container. The ratio of metal elements in hydrogels can be controlled by changing the proportion of metal salts.

The Pt aerogel was prepared in this way: a 0.2 mM Pt metal salt precursor was added into 395 mL deionized water and stirred for 10 min. Then, 5 mL of fresh 80 mM $NaBH_4$ solution was injected into the metallic salt solution, and the mixed solution was stirred for 30 min. Finally, the solution was settled down for gelation for about 2 days. The Pd hydrogel was prepared in the same way, while the obtained mixed solution was settled for about 12 h.

The obtained hydrogels were exchanged with water for 6–8 times, then exchanged with absolute ethanol for at least 9 times to gain an anhydrous atmosphere. The resulting wet gels were transferred into a critical point dryer, and liquid CO_2 was used as medium for the supercritical drying. Finally, the dry aerogels were taken.

3.3. Apparatus

XRD was performed on a Rigaku SmartLab X-ray diffractometer operated at 40 kV and 40 mA with Cu-K_α radiation (λ = 1.5405 Å). The data were collected in the 2θ ranges of 10–90° with a step size of 10°. TEM and EDS were carried out on a Bruker Nano GmbH (Germany) Quantax transmission electron microscope operated at 120 kV. XPS was carried out on a Thermo Fisher Scientific instrument with a mono Al K_α source (hν = 1486.6 eV). Charging effect-induced peak shifts were corrected using the binding energy (BE) of the C1s peak of the substrate (284.8 eV). To estimate the d-band center of the aerogels, the following equation was used [27]:

$$\varepsilon_d = \frac{\int N(\varepsilon)\varepsilon d\varepsilon}{\int N(\varepsilon) d\varepsilon}$$

where N(ε) is the intensity of the surface valance band spectra after Shirley background correction. The surface valance band spectra were collected by XPS.

The nitrogen physisorption isotherm of the Pt aerogel was measured at 77 K on a Quantachrome Autosorb iQ2 instrument via the same process as reported in the literature [30]. About 50 mg of the as-prepared aerogel sample was transferred into the measuring cell and degassed overnight at 323 K under vacuum before measurement. The specific surface area was calculated by using the multipoint Brunauer–Emmett–Teller (BET) equation ($0.05 < P/P_0 < 0.3$), and the pore size distribution was determined from the isotherm using the Barrett–Joyner–Halenda (BJH) theory from the desorption branch. Pore volume was obtained for pores smaller than about 140 nm. BET surface areas and cumulative pore volumes of other Pt_xPd_y aerogels were cited from the literature [30].

3.4. Electrochemical Performance Tests

The electrochemical performance of the prepared catalysts was studied by using a CHI760E electrochemical station (Chenhua Instruments Co., Ltd., Shanghai, China) in a standard three-electrode electrolytic system including a Pt foil (1 cm × 1 cm) counter electrode, a Ag/AgCl (3.0 M KCl) reference electrode, and a glassy carbon working electrode (GCE, 3 mm in diameter). All the electrochemical experiments used 20 mL 0.1 M PBS as electrolyte.

Typically, all the electrochemical catalytic inks were prepared by the following steps: First, 1.0 mg catalyst aerogels were dispersed in 1.0 mL water. Then the mixture was ultrasonicated for 45–90 min to create a stable homogeneous black solution. After that, the solution was further diluted nearly 117.6 times (42.5 µL ink was diluted with 4957.5 µL water). Finally, the ink was stored in the refrigerator (4 °C) for 12 h. Before modification, the GCEs were polished with a 0.3 µm alumina slurry. Then, the GCEs were successively ultrasonicated in deionized water, absolute ethanol, and deionized water. Finally, they were blown dry by nitrogen stream to create a mirrorlike surface. Modified working electrodes

were prepared by simply dropping coating 4 μL ink, which had been ultrasonicated again for 20 min onto the cleaned GCE surface, followed by drying up in air.

Before every electrochemical test, PBS electrolyte was bubbled with N_2 flow for about 30 min to get N_2-saturated electrolyte. The modified working electrode was scanned from −0.64 to 0.96 V (vs. Ag/AgCl, scan speed: 50 mV s^{-1}) in N_2-saturated PBS until stable cyclic voltammetry (CV) response was obtained.

4. Conclusions

In conclusion, a series of Pt_xPd_y bimetallic aerogel and Pt, Pd monometallic aerogel-based electrochemical sensors for the direct determination of H_2O_2 were developed. The catalytic performance of Pt_xPd_y aerogels shows volcano-type behavior with the increase in Pd. The "volcano top": $Pt_{50}Pd_{50}$ aerogel showed the highest sensitivity of 0.19 mA mM^{-1} cm^{-2}, a broad linear range of 5.1–3190 μM, and a lower detection limit of 2.21 μM. Compared with the sensors based on the composite of Pt–Pd and supporting materials, the $Pt_{50}Pd_{50}$ aerogel sensor showed much lower overpotential and a generally wider linear range. The superiority of the $Pt_{50}Pd_{50}$ aerogel sensor can be ascribed to the synergetic bimetallic effect aroused by the introduction of the second metal, which tailors the electronic properties of the catalyst and abundant catalytic sites, fast electron transfer, and superior mass transportability provided by the self-supported 3D porous network structure of the metal aerogel. This work demonstrates the merit of bimetallic effects and the advanced porous structure of metal aerogels, frees the nanocatalysts of substrate materials, and extends the application field of noble metal aerogels.

Supplementary Materials: The following supporting information can be downloaded at: https://www.mdpi.com/article/10.3390/catal12050528/s1, Figure S1: Histograms of TEM ligaments sizes of (a) Pd, (b) Pt, (c) Pt20Pd80, (d) Pt50Pd50, (e) Pt80Pd20 aerogels; Figure S2: Responses of Pt50Pd50 aerogel sensor of continuous addition of 2 mM (50 μL) H2O2 into 20 mL N2-satuated PBS; Figure S3: The effect of different scan rates (30 mV s−1, 50 mV s−1, 70 mV s−1, 100 mV s−1, 200 mV s^{-1}) on the cathodic current of H_2O_2 on $Pt_{20}Pd_{80}$ aerogel. The inset picture was the linear regression of reduction currents and square root of the scan rate, the linear regression equation is $Y = -0.98X - 10.02$, $R^2 = 0.994$.

Author Contributions: Conceptualization, W.L.; methodology, C.P. and Y.Z.; validation, J.Y., D.L. and J.L.; formal analysis, C.P.; investigation, C.P. and Y.S.; resources, W.L.; data curation, C.P.; writing—original draft preparation, C.P., Y.S. and W.L.; writing—review and editing, W.L.; visualization, C.P; supervision, W.L.; project administration, W.L.; funding acquisition, W.L. All authors have read and agreed to the published version of the manuscript.

Funding: This research was funded by financial support from the National Natural Science Foundation of China, grant number 52173296; the Natural Science Foundation of Guangdong Province (China), grant number 2022A1515011826, and 100 Top Talents Program—Sun Yat-sen University (China).

Data Availability Statement: Data are contained within the article.

Acknowledgments: Financial support from the National Natural Science Foundation of China (52173296), the Natural Science Foundation of Guangdong Province (China) (2022A1515011826), and the 100 Top Talents Program—Sun Yat-sen University (China) is gratefully acknowledged.

Conflicts of Interest: The authors declare no conflict of interest.

References

1. Jiao, L.; Xu, W.; Yan, H.; Wu, Y.; Liu, C.; Du, D.; Lin, Y.; Zhu, C. Fe–N–C single-atom nanozymes for the intracellular hydrogen peroxide detection. *Anal. Chem.* **2019**, *91*, 11994–11999. [CrossRef] [PubMed]
2. Shi, L.; Wang, Y.; Zhang, C.; Zhao, Y.; Lu, C.; Yin, B.; Yang, Y.; Gong, X.; Teng, L.; Liu, Y.; et al. An acidity-unlocked magnetic nanoplatform enables self-boosting ROS generation through upregulation of lactate for imaging-guided highly specific chemodynamic therapy. *Angew. Chem. Int. Ed.* **2021**, *60*, 9562–9572. [CrossRef] [PubMed]
3. Campos-Martin, J.M.; Blanco-Brieva, G.; Fierro, J.L. Hydrogen peroxide synthesis: An outlook beyond the anthraquinone process. *Angew. Chem. Int. Ed.* **2006**, *45*, 6962–6984. [CrossRef] [PubMed]

4. Perry, S.C.; Pangotra, D.; Vieira, L.; Csepei, L.-I.; Sieber, V.; Wang, L.; Ponce de León, C.; Walsh, F.C. Electrochemical synthesis of hydrogen peroxide from water and oxygen. *Nat. Rev. Chem.* **2019**, *3*, 442–458. [CrossRef]
5. Melchionna, M.; Fornasiero, P.; Prato, M. The rise of hydrogen peroxide as the main product by metal-free catalysis in oxygen reductions. *Adv. Mater.* **2019**, *31*, 1802920. [CrossRef]
6. Ishikawa, K.; Takenaga, K.; Akimoto, M.; Koshikawa, N.; Yamaguchi, A.; Imanishi, H.; Nakada, K.; Honma, Y.; Hayashi, J.-I. Ros-generating mitochondrial DNA mutations can regulate tumor cell metastasis. *Science* **2008**, *320*, 661–664. [CrossRef]
7. Cheng, C.; Zhang, C.; Gao, X.; Zhuang, Z.; Du, C.; Chen, W. 3D network and 2D paper of reduced graphene oxide/Cu_2O composite for electrochemical sensing of hydrogen peroxide. *Anal. Chem.* **2018**, *90*, 1983–1991. [CrossRef]
8. Meier, J.; Hofferber, E.M.; Stapleton, J.A.; Iverson, N.M. Hydrogen peroxide sensors for biomedical applications. *Chemosensors* **2019**, *7*, 64. [CrossRef]
9. Tantawi, O.; Baalbaki, A.; El Asmar, R.; Ghauch, A. A rapid and economical method for the quantification of hydrogen peroxide (H_2O_2) using a modified HPLC apparatus. *Sci. Total Environ.* **2019**, *654*, 107–117. [CrossRef]
10. Trujillo, R.M.; Barraza, D.E.; Zamora, M.L.; Cattani-Scholz, A.; Madrid, R.E. Nanostructures in hydrogen peroxide sensing. *Sensors* **2021**, *21*, 2204. [CrossRef]
11. Han, T.; Zhang, Y.; Xu, J.; Dong, J.; Liu, C.-C. Monodisperse AuM (M = Pd, Rh, Pt) bimetallic nanocrystals for enhanced electrochemical detection of H_2O_2. *Sens. Actuators B* **2015**, *207*, 404–412. [CrossRef]
12. Sun, Y.; Luo, M.; Meng, X.; Xiang, J.; Wang, L.; Ren, Q.; Guo, S. Graphene/intermetallic PtPb nanoplates composites for boosting electrochemical detection of H_2O_2 released from cells. *Anal. Chem.* **2017**, *89*, 3761–3767. [CrossRef] [PubMed]
13. Bian, T.; Liu, H.; Sun, B.; Xiao, B.; Jiang, Y.; Jin, C.; Yuan, A.; Zhang, H.; Yang, D. Ion-templated fabrication of Pt-Cu alloy octahedra with controlled compositions for electrochemical detection of H_2O_2. *J. Alloys Compd.* **2019**, *788*, 1334–1340. [CrossRef]
14. Liu, W.; Hiekel, K.; Hübner, R.; Sun, H.; Ferancova, A.; Sillanpää, M. Pt and Au bimetallic and monometallic nanostructured amperometric sensors for direct detection of hydrogen peroxide: Influences of bimetallic effect and silica support. *Sens. Actuators B* **2018**, *255*, 1325–1334. [CrossRef]
15. Liu, Y.; Li, H.; Gong, S.; Chen, Y.; Xie, R.; Wu, Q.; Tao, J.; Meng, F.; Zhao, P. A novel non-enzymatic electrochemical biosensor based on the nanohybrid of bimetallic PdCu nanoparticles/carbon black for highly sensitive detection of H_2O_2 released from living cells. *Sens. Actuators B* **2019**, *290*, 249–257. [CrossRef]
16. Wu, L.; Yin, W.; Tan, X.; Wang, P.; Ding, F.; Zhang, H.; Wang, B.; Zhang, W.; Han, H. Direct reduction of $HAuCl_4$ for the visual detection of intracellular hydrogen peroxide based on Au-Pt/SiO_2 nanospheres. *Sens. Actuators B* **2017**, *248*, 367–373. [CrossRef]
17. Sun, Y.; Luo, M.; Qin, Y.; Zhu, S.; Li, Y.; Xu, N.; Meng, X.; Ren, Q.; Wang, L.; Guo, S. Atomic-thick PtNi nanowires assembled on graphene for high-sensitivity extracellular hydrogen peroxide sensors. *ACS Appl. Mater. Interfaces* **2017**, *9*, 34715–34721. [CrossRef] [PubMed]
18. Bai, Z.; Dong, W.; Ren, Y.; Zhang, C.; Chen, Q. Preparation of nano Au and Pt alloy microspheres decorated with reduced graphene oxide for nonenzymatic hydrogen peroxide sensing. *Langmuir* **2018**, *34*, 2235–2244. [CrossRef]
19. Ferrando, R.; Jellinek, J.; Johnston, R.L. Nanoalloys: From theory to applications of alloy clusters and nanoparticles. *Chem. Rev.* **2008**, *108*, 845–910. [CrossRef]
20. Gesser, H.D.; Goswami, P.C. Aerogels and related porous materials. *Chem. Rev.* **1989**, *89*, 765–788. [CrossRef]
21. Cai, B.; Dianat, A.; Hubner, R.; Liu, W.; Wen, D.; Benad, A.; Sonntag, L.; Gemming, T.; Cuniberti, G.; Eychmuller, A. Multimetallic hierarchical aerogels: Shape engineering of the building blocks for efficient electrocatalysis. *Adv. Mater.* **2017**, *29*, 1605254. [CrossRef] [PubMed]
22. Liu, W.; Herrmann, A.K.; Bigall, N.C.; Rodriguez, P.; Wen, D.; Oezaslan, M.; Schmidt, T.J.; Gaponik, N.; Eychmuller, A. Noble metal aerogels-synthesis, characterization, and application as electrocatalysts. *Acc. Chem. Res.* **2015**, *48*, 154–162. [CrossRef] [PubMed]
23. Jiang, X.; Du, R.; Hübner, R.; Hu, Y.; Eychmüller, A. A roadmap for 3D metal aerogels: Materials design and application attempts. *Matter* **2021**, *4*, 54–94. [CrossRef]
24. Du, R.; Fan, X.; Jin, X.; Hübner, R.; Hu, Y.; Eychmüller, A. Emerging noble metal aerogels: State of the art and a look forward. *Matter* **2019**, *1*, 39–56. [CrossRef]
25. Cai, B.; Eychmuller, A. Promoting electrocatalysis upon aerogels. *Adv. Mater.* **2019**, *31*, 1804881. [CrossRef]
26. Dubale, A.A.; Zheng, Y.; Wang, H.; Hubner, R.; Li, Y.; Yang, J.; Zhang, J.; Sethi, N.K.; He, L.; Zheng, Z.; et al. High-performance bismuth-doped nickel aerogel electrocatalyst for the methanol oxidation reaction. *Angew. Chem. Int. Ed.* **2020**, *59*, 13891–13899. [CrossRef]
27. Zheng, Y.; Yang, J.; Lu, X.; Wang, H.; Dubale, A.A.; Li, Y.; Jin, Z.; Lou, D.; Sethi, N.K.; Ye, Y.; et al. Boosting both electrocatalytic activity and durability of metal aerogels via intrinsic hierarchical porosity and continuous conductive network backbone preservation. *Adv. Energy Mater.* **2020**, *11*, 2002276. [CrossRef]
28. Liu, W.; Herrmann, A.K.; Geiger, D.; Borchardt, L.; Simon, F.; Kaskel, S.; Gaponik, N.; Eychmuller, A. High-performance electrocatalysis on palladium aerogels. *Angew. Chem. Int. Ed.* **2012**, *51*, 5743–5747. [CrossRef]
29. Du, R.; Jin, W.; Wu, H.; Hübner, R.; Zhou, L.; Xue, G.; Hu, Y.; Eychmüller, A. Rapid synthesis of gold–palladium core–shell aerogels for selective and robust electrochemical CO_2 reduction. *J. Mater. Chem. A Chem.* **2021**, *9*, 17189–17197. [CrossRef]

30. Liu, W.; Rodriguez, P.; Borchardt, L.; Foelske, A.; Yuan, J.; Herrmann, A.K.; Geiger, D.; Zheng, Z.; Kaskel, S.; Gaponik, N.; et al. Bimetallic aerogels: High-performance electrocatalysts for the oxygen reduction reaction. *Angew. Chem. Int. Ed.* **2013**, *52*, 9849–9852. [CrossRef]
31. Liu, W.; Haubold, D.; Rutkowski, B.; Oschatz, M.; Hübner, R.; Werheid, M.; Ziegler, C.; Sonntag, L.; Liu, S.; Zheng, Z.; et al. Self-supporting hierarchical porous PtAg alloy nanotubular aerogels as highly active and durable electrocatalysts. *Chem. Mater.* **2016**, *28*, 6477–6483. [CrossRef]
32. Wen, D.; Liu, W.; Haubold, D.; Zhu, C.; Oschatz, M.; Holzschuh, M.; Wolf, A.; Simon, F.; Kaskel, S.; Eychmuller, A. Gold aerogels: Three-dimensional assembly of nanoparticles and their use as electrocatalytic interfaces. *ACS Nano* **2016**, *10*, 2559–2567. [CrossRef] [PubMed]
33. Zhang, G.; Shao, Z.-G.; Lu, W.; Xie, F.; Qin, X.; Yi, B. Electrochemical preparation and characterization of PdPt nanocages with improved electrocatalytic activity toward oxygen reduction reaction. *Electrochim. Acta* **2013**, *103*, 66–76. [CrossRef]
34. Luo, M.; Guo, S. Strain-controlled electrocatalysis on multimetallic nanomaterials. *Nat. Rev. Chem.* **2017**, *2*, 17095. [CrossRef]
35. Veisz, B.; Tóth, L.; Teschner, D.; Paál, Z.; Győrffy, N.; Wild, U.; Schlögl, R. Palladium-platinum powder catalysts manufactured by colloid synthesis. *J. Mol. Catal. A Chem.* **2005**, *238*, 56–62. [CrossRef]
36. Ruban, A.; Hammer, B.; Stoltze, P.; Skriver, H.L.; Nørskov, J.K. Surface electronic structure and reactivity of transition and noble metals1communication presented at the first francqui colloquium. *J. Mol. Catal. A Chem.* **1997**, *115*, 421–429. [CrossRef]
37. Gao, D.; Arán-Ais, R.M.; Jeon, H.S.; Roldan Cuenya, B. Rational catalyst and electrolyte design for CO_2 electroreduction towards multicarbon products. *Nat. Catal.* **2019**, *2*, 198–210. [CrossRef]
38. Yang, Y.; Zhang, H.; Wang, J.; Yang, S.; Liu, T.; Tao, K.; Chang, H. A silver wire aerogel promotes hydrogen peroxide reduction for fuel cells and electrochemical sensors. *J. Mater. Chem. A Chem.* **2019**, *7*, 11497–11505. [CrossRef]
39. Sha, R.; Vishnu, N.; Badhulika, S. Bimetallic Pt-Pd nanostructures supported on MoS_2 as an ultra-high performance electrocatalyst for methanol oxidation and nonenzymatic determination of hydrogen peroxide. *Microchim. Acta.* **2018**, *185*, 399. [CrossRef]
40. Chen, K.J.; Chandrasekara Pillai, K.; Rick, J.; Pan, C.J.; Wang, S.H.; Liu, C.C.; Hwang, B.J. Bimetallic PtM (M=Pd, Ir) nanoparticle decorated multi-walled carbon nanotube enzyme-free, mediator-less amperometric sensor for H_2O_2. *Biosens. Bioelectron.* **2012**, *33*, 120–127. [CrossRef]
41. Fu, Y.; Huang, D.; Li, C.; Zou, L.; Ye, B. Graphene blended with SnO_2 and Pd-Pt nanocages for sensitive non-enzymatic electrochemical detection of H_2O_2 released from living cells. *Anal. Chim. Acta.* **2018**, *1014*, 10–18. [CrossRef]
42. Li, H.; Zhao, H.; He, H.; Shi, L.; Cai, X.; Lan, M. Pt-Pd bimetallic nanocoral modified carbon fiber microelectrode as a sensitive hydrogen peroxide sensor for cellular detection. *Sens. Actuators B* **2018**, *260*, 174–182. [CrossRef]
43. Qi, H.; Song, J.; Fu, Y.; Wu, X.; Qi, H. Highly dispersive Pt-Pd nanoparticles on graphene oxide sheathed carbon fiber microelectrodes for electrochemical detection of H_2O_2 released from living cells. *Nanotechnology* **2020**, *31*, 135503. [CrossRef]
44. Sun, X.; Guo, S.; Liu, Y.; Sun, S. Dumbbell-like PtPd -Fe_3O_4 nanoparticles for enhanced electrochemical detection of H_2O_2. *Nano Lett.* **2012**, *12*, 4859–4863. [CrossRef]
45. Tian, L.; Chen, Y.; Wu, S.; Cai, Y.; Liu, H.; Zhang, J.; Yang, C.; He, G.; Xiao, W.; Li, L.; et al. One-pot synthesis of cubic PtPdCu nanocages with enhanced electrocatalytic activity for reduction of H_2O_2. *RSC Adv.* **2017**, *7*, 34071–34076. [CrossRef]
46. Zhu, D.; Zuo, J.; Tan, L.; Pang, H.; Ma, H. Enzymeless electrochemical determination of hydrogen peroxide at a heteropolyanion-based composite film electrode. *New J. Chem.* **2019**, *43*, 1053–1062. [CrossRef]
47. Zhang, Y.; Zhang, C.; Zhang, D.; Ma, M.; Wang, W.; Chen, Q. Nano-assemblies consisting of Pd/Pt nanodendrites and poly (diallyldimethylammonium chloride)-coated reduced graphene oxide on glassy carbon electrode for hydrogen peroxide sensors. *Mater. Sci. Eng. C* **2016**, *58*, 1246–1254. [CrossRef]
48. Sun, Y.; Zheng, H.; Wang, C.; Yang, M.; Zhou, A.; Duan, H. Ultrasonic-electrodeposition of PtPd alloy nanoparticles on ionic liquid-functionalized graphene paper: Towards a flexible and versatile nanohybrid electrode. *Nanoscale* **2016**, *8*, 1523–1534. [CrossRef]